Redox Biology 51 (2022) 102262

Contents lists available at ScienceDirect

Redox Biology

journal homepage: www.elsevier.com/locate/redox

# ACSL4 deficiency confers protection against ferroptosis-mediated acute kidney injury

Yue Wang [a,b,1], Menghan Zhang [a,c,1], Ran Bi [a,1], Yali Su [a], Fei Quan [a], Yanting Lin [a], Chongxiu Yue [a], Xinmeng Cui [a], Qixiang Zhao [a], Siliang Liu [a], Yong Yang [a], Dayong Zhang [d], Qiuhua Cao [a,**], Xinghua Gao [a,*]

[a] Center for New Drug Safety Evaluation and Research, State Key Laboratory of Natural Medicines, China Pharmaceutical University, Nanjing, Jiangsu, 211198, PR China
[b] Department of Endocrinology, The Second Affiliated Hospital of Anhui Medical University, Hefei, 230601, China
[c] Eshelman School of Pharmacy, The University of North Carolina at Chapel Hill, Chapel Hill, NC, 27599-7568, USA
[d] School of Sciences, China Pharmaceutical University, Nanjing, 211198, China

ARTICLE INFO

*Keywords:*
ACSL4
Acute kidney injury
Ferroptosis
Macrophages
HIF-1α

ABSTRACT

The term ferroptosis coined in 2012 causes acute kidney injury (AKI). However, its pathway mechanism in AKI is poorly understood. In this study, we conducted an RNA-sequence analysis of kidneys in AKI and normal mice to explore the pathway mechanism of ferroptosis. Consequently, differentially expressed genes highlighted Acyl-CoA synthetase long-chain family (ACSL4), a known promotor for ferroptosis. Besides, RT-PCR, Western blot, and immunohistochemical analyses confirmed its upregulation. HIF-1α was downregulated in I/R-AKI mice, and in vitro studies confirmed a negative regulation of HIF-1α on ACSL4. To explore the role of ACSL4 in AKI, we constructed ACSL4 knockout in kidney tubules of mice-as Cdh16Cre-ACSL4$^{F/F}$ mice. Results revealed that ACSL4 knockout significantly reduced ferroptosis and inhibited the functional and pathological injury of AKI mice. Meanwhile, the kidneys of Cdh16Cre-ACSL4$^{F/F}$ mice demonstrated a significantly decreased inflammation and macrophage infiltration. Further, additional explorations were explored to decipher a more thorough understanding of ferroptotic immunogenicity. As a result, neutrophils were not directly recruited by ferroptotic cells, but by ferroptotic cell-induced macrophages. Further, ACSL4 inhibitor rosiglitazone significantly inhibited AKI. Collectively, these data provide novel insights into the AKI pathogenesis, and defined ACSL4 as an effective target in AKI.

## 1. Introduction

The prevalence of acute kidney injury (AKI) is increasing across the globe, with mortality of above 2 million people annually [1,2]. AKI patients are associated with complications, like chronic kidney disease (CKD), increasing mortality [3,4]. The current treatment interventions for AKI include adequate hydration, adequate blood volume circulation, and preventing nephrotoxins [5]. So far, no effective pharmacologic strategy for AKI prevention and treatment has been reported. Thus, to improve clinical outcomes, it is necessary to identify key molecules involved in AKI.

Renal tubular cell death is the hallmark in AKI [6]. Several types of cell death-like apoptosis, necrosis, and pyroptosis have been considered pathophysiologic relevant in AKI [7]. Apoptosis has been detected in several AKI models, and apoptotic regulators including Bcl-2 and caspases have been shown in AKI models [8,9]. A critical role of necrosis in AKI was first suggested in 2012 [10], and subsequently confirmed by scholars [11,12]. Pyroptosis, a strong inflammatory form of cell death, is also considered a major cause of septic AKI, cisplatin-induced AKI, and I/R-AKI [13–15]. However, no drug has been shown to effectively halt AKI, and potent pharmacodynamic targets have not been identified. Therefore, a new understanding of the pathology of AKI is urgent needed. With the deepening knowledge of cell death, ferroptosis was identified in 2012 as an iron-dependent necrotic form [16]. Research has

* Corresponding author. China Pharmaceutical University, Nanjing, China.
** Corresponding author.
*E-mail addresses:* 1520210058@cpu.edu.cn (Q. Cao), gaoxinghua@cpu.edu.cn (X. Gao).
[1] These authors equally contributed to this work.

https://doi.org/10.1016/j.redox.2022.102262
Received 24 January 2022; Accepted 7 February 2022
Available online 9 February 2022

confirmed that it participates in various diseases, among them carcinoma, neurodegenerative diseases, AKI, and I/R injury [17]. Previous studies indicate that ferroptosis but not necrosis promote I/R-AKI and oxalate nephropathy [18]. Besides, ferroptosis is involved in the AKI model induced by folic acid (FA) [19]. At present, ferroptosis is a potential therapeutic target for AKI [20,21]. Our previous study found that quercetin potentially alleviates AKI by inhibiting ferroptosis [22]. VDR activation attenuates cisplatin-induced AKI by inhibiting ferroptosis [23]. XJB-5-131 suppresses I/R damage with a mechanism related to ferroptosis of tubular cells [24]. However, the molecular mechanism underlying ferroptosis in AKI is largely understudied.

Ferroptosis is characterized by iron-dependent lipid peroxide accumulation. ACSL4, an enzyme that converts fatty acid to fatty *acyl-CoA* esters, regulates lipid biosynthesis. Notably, Hua Yuan et al. discovered that ACSL4 contributes to ferroptosis [25], while Sebastian Doll et al. used CRISPR-based genetic screening and analysis of resistant cells confirmed ACSL4 as a key player in ferroptosis [26]. While the important role of ACSL4 in ferroptosis remains known, its role in AKI is unclear. Herein, Cdh16Cre-ACSL4$^{F/F}$ mice and ACSL4 inhibitor rosiglitazone were used to assess the role of ACSL4 in AKI. ACSL4 knockout alleviates kidney injury by inhibiting ferroptosis and inflammation. As such, targeting ACSL4 or related regulated molecular is a therapeutic strategy for AKI.

## 2. Materials and methods

### 2.1. Cell lines

Dr. Chunsun Dai provided the NRK-52E Cells, and HK-2 cells were purchased from China Cell Bank. The cells were cultured in DMEM/Ham's F12 (BI) supplemented with 5% fetal bovine serum (BI). An immortalized macrophage line (iBMDM) derived from C57BL/6 mice was provided by Dr. Feng Shao, which was widely used in Dr. Shao's previous studies [27–29]. Dr. Shao got this cell from K. A. Fitzgerald (University of Massachusetts Medical School, United States), who generated this cell line using J2 recombinant retrovirus (carrying v-myc and v-raf/mil oncogenes) [30]. The iBMDM cells were cultured with DMEM (Gibco). All the cells were maintained with 5% CO2 in a 37 °C incubator.

### 2.2. Cell viability assay

Cells were cultured in 96-well plates and treated with drugs at the indicated time. Cell viability was detected using the sulforhodamine B (SRB) assay [31,32].

### 2.3. Drug treatment

The following reagents were used for in vitro experiments: Erastin (Era) and RSL3 (MedChemExpress, cat number: HY-15763 and HY-100218A), Bay-87-2243 (Selleck, cat number: 1227158-85-1) and PT-2385 (Selleck, cat number: 1672665-49-4). The following were used for in vivo experiments; 5 mg/kg Fer-1 (Aladdin, cat number: Q111273 or F129882), 0.5 mg/kg rosiglitazone (Aladdin, cat number: 302543-62-0), and 200 mg/kg FA (Aladdin, cat number: F103641).

### 2.4. Mice

This study used male C57BL/6J mice (7–8 weeks). The mice were housed in a 12 h/12 h light/dark cycle. ACSL4 (NCBI reference sequence: NM_001033600.1; MGI link: http://www.informatics.jax.org/marker/MGI:1354713; Gene ID: 50790(NCBI); Ensembl: ENSMUST00000033634.4) floxP mice, generated using CRISPR/Cas9, were obtained from Southern Model Animal Center (Shanghai, China), as well as the Cdh16-cre mice. The generation of ACSL4-KO mice uses the principle of homologous recombination and the method of homologous recombination of fertilized eggs to modify the Acsl4 gene by flox. The brief process was as follows: Cas9 mRNA and gRNA were obtained by in vitro transcription. Homologous recombination vector was constructed by the in-fusion cloning method, which contains a 4.0 kb 5′ homology arm, a 0.8 kb flox region, and a 4.0 kb 3′ homology arm. The Cas9 mRNA, gRNA, and donor vectors were microinjected into the fertilized eggs of C57BL/6J mice. The ACSL4F/F mouse was mated with a mouse that specifically expresses Cdh16-Cre recombinase in the kidney, leading to renal tubule knockout of ACSL4. The tails of the mice were genotyped using PCR; then sequence analysis was conducted. All animal experiments were performed as per the National Institutes of Health Guide for the Care and Use of Laboratory Animals and approved by the Center for New Drug Safety Evaluation and Research, China Pharmaceutical University.

### 2.5. Animal models

#### 2.5.1. Renal ischemia/reperfusion model

The mice were randomly divided into different groups with 6 mice in each group. Briefly, 5 mg/kg Fer-1 (Aladdin, cat number: Q111273 or F129882) and 0.5 mg/kg rosiglitazone (Aladdin, cat number: 302543-62-0) were administrated 30 min before the ischemic operation through i.p. injection and i.v. injection respectively. The Renal ischemia/reperfusion was induced in the following procedure: The mouse prone was placed on the heated surface covered with an absorbent bench pad. The legs were tapped to the surgical surface. The dorsal skin along the midline of the mouse (approximately 1.5 cm) was cut using scissors and forceps. A small incision was made through the bilateral flank muscle and fascia above the kidney and exteriorize the kidney. Then the mice were ischemic for 30 min by clamping the bilateral renal pedicle respectively, and moving the nontraumatic clamps. The sham group was only done with the sham operation, but no ischemia. Mice were sacrificed after 24 h and blood samples and kidneys were collected. The right kidney was half snap-frozen and half fixed in 4% phosphate-buffered formaldehyde. The left kidney was isolated to obtain kidney immune cells for flow cytometry analysis.

#### 2.5.2. Folic acid (FA)-induced AKI model

FA was dissolved in 0.3 mol/L NaHCO3, then was i.p. injected to mice at the dose of 200 mg/kg. After 24 h, the mice were sacrificed. Tissues were kept for subsequent examination.

### 2.6. RNA-seq profiling

The RNA-sequencing was performed in Novogene as described before [22]. Briefly, a Trizol reagent was used to isolate the RNA of kidney tissue. RNA (3 μg) per sample was used for RNA sample preparations. NEBNext® UltraTM RNA Library Prep Kit for Illumina® (NEB, USA) was used for sequencing libraries as per the manufacturer's recommendations. Transcripts expression with $|\text{Log2 Fc}| > 1.5$, adjusted $P\text{-value} < 0.05$ were considered statistically significant. The RNA sequencing data file was uploaded to the public GEO databases (GSE181842).

### 2.7. Real-time PCR analysis

Total RNA from tissues or cells were extracted using Trizol reagent (Invitrogen, cat number: 15596026), and reverse transcribed into cDNA using a cDNA synthesis kit (Takara, cat number: RR047A). Quantitative PCR was done with a Step one plus Real-Time PCR system (Applied

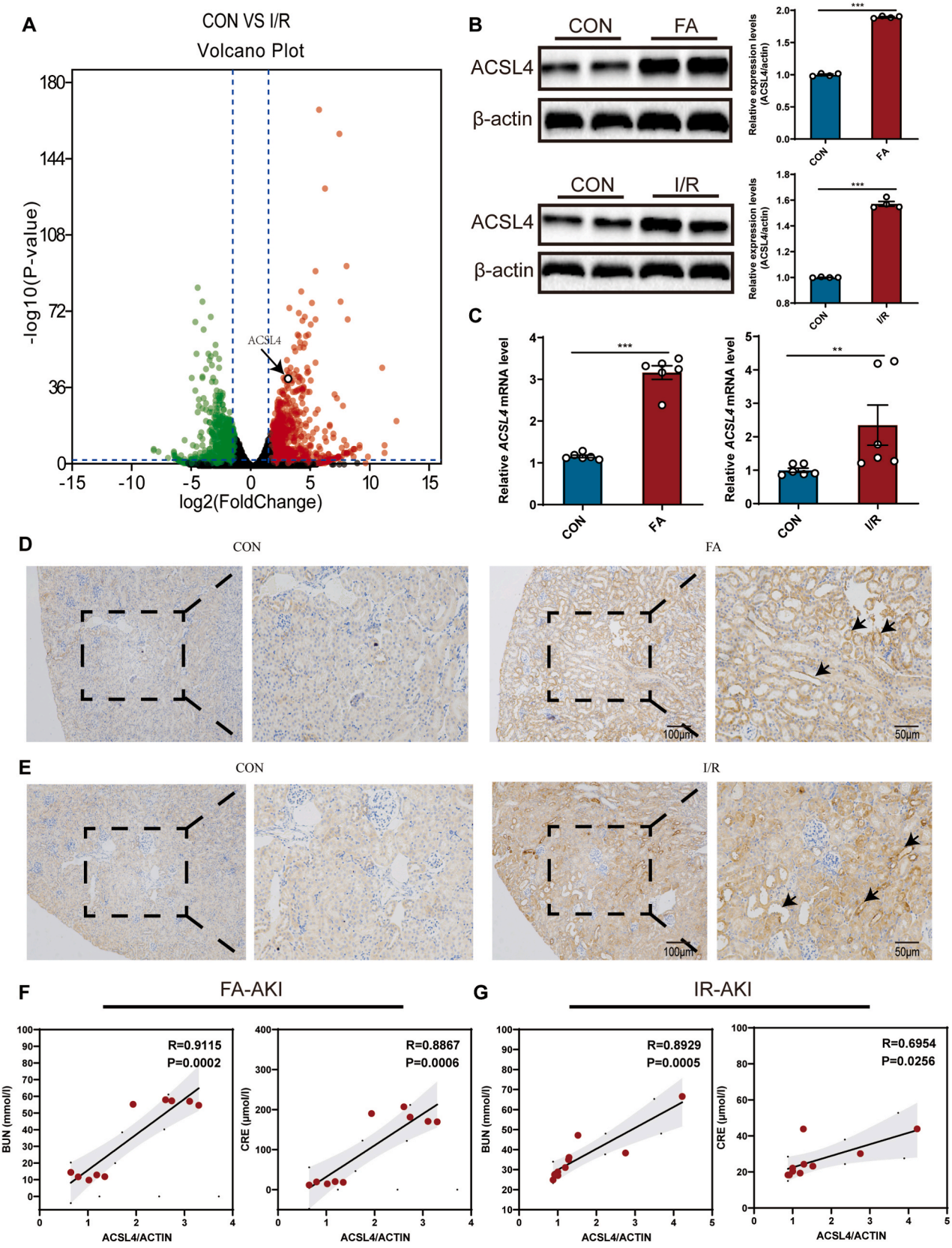


**Fig. 1.** Up-regulation of ACSL4 in AKI. (A) The RNA-seq volcano graphs of the CON and I/R-induced AKI groups. N=3. (B) ACSL4 protein expression in AKI detected by WB. N=4. (C) The expression levels of *ACSL4* mRNA after AKI detection by RT-PCR, N=6. (D–E) Representative images showing ACSL4 expression detected by immunohistochemistry. Black arrows indicate ACSL4 expression. The scale bar represents 50 μm. (F–G) Correlation analysis of ACSL4 mRNA levels and kidney function indicator BUN or blood CRE levels in mice. The Pearson correlation statistic test was used for data analysis. N=10. $^{**}p < 0.01$, $^{***}p < 0.001$, compared to the CON group.

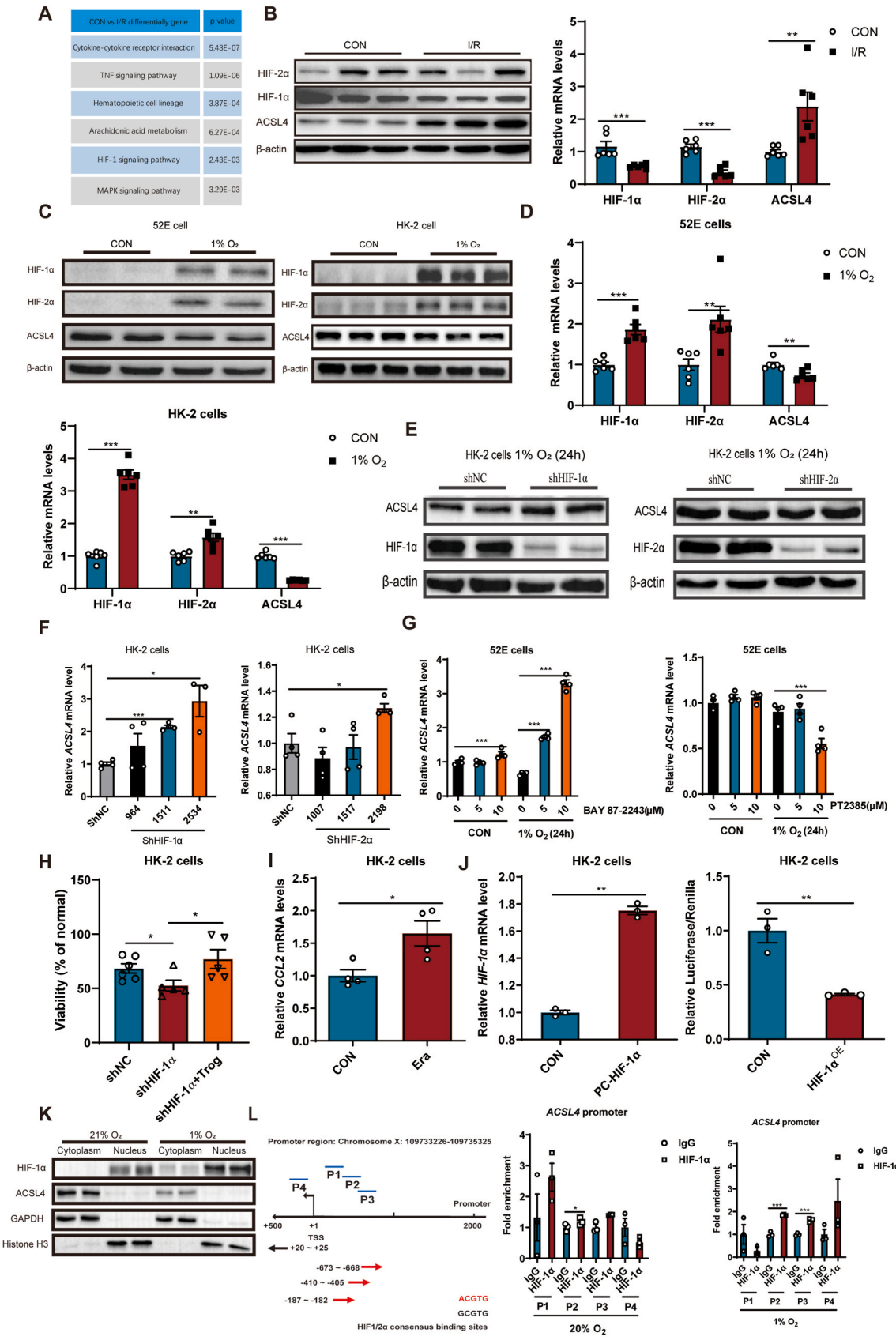


-

*(caption on next page)*

**Fig. 2.** HIF-1α binds to the ACSL4 promoter and negatively regulates ACSL4. All the cells in the hypoxia environment were cultured for 24 h. (A) A table summarizing the results of the RNA-seq data in CON and I/R groups obtained via gene ontology. N=3. (B) WB and RT-PCR results of HIF-1α, HIF-2α, ACSL4 in I/R-induced AKI kidney tissues. N=6. (C)Protein expression levels of HIF-1α, HIF-2α, ACSL4 determined in 52E and HK-2 cells after culturing cells in 1% $O_2$ hypoxia for 24 h. N=3. (D) RT-PCR results of *HIF-1α*, *HIF-2α,* and *ACSL4* in 52E and HK-2 cells. N=3. (E) The HIF-1α and HIF-2α knockdown of HK-2 cells cultured under 1% $O_2$ hypoxia for 24 h and WB results showing the expression of HIF-1α, HIF-2α, and ACSL4. N=3. (F, G) RT-PCR results showing the expression of *ACSL4* after knockdown of HIF-1α, HIF-2α or after treatment with HIF-1α inhibitor BAY 87–2243 (10 μM) or HIF-2α inhibitor PT2385 (10 μM) for 24 h. N=3. (H) The cell viability detected by SRB after the knockdown of HIF-1α treated with Erastin (1 μM). Troglitazone (1 μM) was added at the same time as Erastin. N=5. (I) RT-PCR results showed the *CCL2* mRNA levels in the treated cells. N=4. (J) RT-PCR results showing the efficiency of HIF-1α overexpression in plasmid transfected into HK-2 cells, and Luciferase results showing the interaction between HIF-1α and ACSL4. N=3. (K) WB results showing the distribution and expression of HIF-1α and ACSL4 in HK-2 cells at 21% $O_2$ and 1% $O_2$. N=3. (L) The database predicting the binding site of HIF-1α and ACSL4. The Chip immunoprecipitation experiments of HK-2 cells showed the binding sites at 20% $O_2$ or 1% $O_2$ (24 h). N=3. $*p < 0.05$, $**p < 0.01$, $***p < 0.001$, compared to CON or shNC groups.

Biosystems, USA) with gene-specific primers. The amount of RNA was calculated using the comparative threshold cycle method. All primers were custom-made by Genscript. The primer sequences are shown in Supplementary Table 1.

### 2.8. Western blotting

The samples were lysed in RIPA buffer containing enzyme-inhibitor complex. Subsequently, the concentration of the protein sample was measured using the Bradford method. Samples were then electrophoresed, and transferred onto PVDF membranes. After blocking for 1 h, the samples were incubated with ACSL4 (Abcam, ab155282, 1:5000), HIF-1α (Abcam, 36169S, 1:1000) or HIF-2α (Abcam, 59973S, 1:1000) at 4 °C overnight. The blots were then incubated with secondary antibodies, and signaling was obtained with chemiluminescence reagents and measured using the Image J software.

### 2.9. Renal function, histology, and immunohistochemistry analyses

Serum creatinine (Nanjing Jiancheng Bioengineering Institute, C011-2-1, Nanjing, China) and BUN (Nanjing Jiancheng Bioengineering Institute, A003-2, Nanjing, China) were two important markers for kidney function 18, and were detected as manufacturer's protocols. Renal injury scores were performed on hematoxylin & eosin stained kidney sections and assessed by a pathologist blinded to the experiment, as described before 22. For immunohistochemistry, antigenic recovery was performed as follows: the slices were placed in 0.01 mol/L pH 6.0 citric acid buffer with a microwave oven on high heat until boiling, then turned to medium heat and kept above 95 °C for 20 min, cooled naturally to room temperature. Then, ACSL4 (1:500, Abcam, ab155282) antibody was used to detect the ACSL4 expression, whereas F4/80 antibody (1:100, Cat No.70076S; CST, USA) and MPO antibody (1:50, Cat No. ab9535; Abcam, UK) was used to detect the macrophages and neutrophils in kidney tissues. All the primary antibodies were added in 10% goat serum in PBST with appropriate concentration at 4 °C overnight. The secondary antibody (HRP secondary antibodies, Cat No. KIT-5002 or KIT-5005; MXB Biotechnologies, China) was added with 10% goat serum in PBST for 1 h at room temperature. An Olympus BX41 microscope was used to obtain images.

### 2.10. Immunofluorescent staining

The kidney of ACSL4F/F and cdh16-Cre/ACSL4F/F mice were snap-frozen in liquid nitrogen and placed in an optimal cutting temperature embedding matrix. Frozen sections (10 μm) were fixed in icy acetone for 10 min then washed using PBS. Then, sections were stained with ACSL4 (1:250, Abcam, ab155282) antibody or Cytokeratin 18 (1:200, Proteintech, 66187-1-Ig) antibody followed by staining of secondary Goat anti-Rabbit IgG (H+L) Cross-Adsorbed Secondary Antibody, Alexa Fluor 488 (Thermo Fisher, A11008), or Goat anti-Mouse IgG (H+L) Highly Cross-Adsorbed Secondary Antibody, Alexa Fluor 633 (Thermo Fisher, A21052), respectively. A Carl Zeiss LSM700 laser confocal microscope was used to obtain images.

Kidney cell death was labeled by TUNEL staining (Beyotime, cat number: C1088) as previously described for details [22,33]. Briefly, the tissue sections were dewaxed using xylene then permeabilized with 0.1% Triton X-100. Sections were then incubated with TUNEL for 1 h at 37 °C, then counterstained with DAPI (Beyotime, cat number: C1005). The FITC-labeled TUNEL-positive cells were imaged under a fluorescent microscope and cells with green fluorescence were defined as tissue cell-death (Carl Zeiss LSM700).

### 2.11. Transfection

Lentiviral HIF-1α or HIF-2α shRNA (Aikande Biological Company, China) were used to transfect HK-2 cells with Polybrene polybrene A at the concentration of 5 μg/ml (Gene-Pharma, Shanghai), as per the manufacturer's instructions.

### 2.12. HIF-1α/ACSL4 dual-luciferase reporter system

The 3′-UTR of the corresponding gene containing HIF-1α binding sites were amplified using overlap PCR and cloned downstream of the dual-luciferase reporter gene assay in the pmirGLO vector. HK-2 cells were transfected with 100 ng reporter plasmids, 100 nmol/L HIF-1α pcDNA3.1-3xFlag-C plasmids, and ACSL4 promoter pGL3-Basic plasmids for 48 h. Subsequently, the cells were assayed using the dual-luciferase reporter gene assay kit (RG-027, Beyotime, Nanjing, China). Dual-luciferase activities were normalized to firefly luciferase activities.

### 2.13. Chromatin immunoprecipitation assay

The HK-2 cells were digested and plated on a 15 cm dish (about $4 \times 10^6$ cells per immunoprecipitation) in 21% $O_2$ and 1% $O_2$ for 24 h. Thereafter, the cells were counted, fixed with formaldehyde, washed using 1 × PBS. SimpleChIP® Plus Enzymatic Chromatin IP Kit (Cell signaling technology, Magnetic Beads, cat number: 9005) was then used for subsequent experiment cell culture cross-linking and sample preparation. The antibodies HIF-1α (Abcam, 36169S, 1:1000), Histone H3 (D2B12) XP® rabbit mAb (ChIP Formulated) 4620 and normal rabbit IgG 2729 in the SimpleChIP® Plus Enzymatic Chromatin IP Kit (Cell signaling technology, Magnetic Beads, cat number: 9005) were used in ChIP experiments. The real-time PCR machine software was used to analyze quantitative PCR results. The signal obtained from each immunoprecipitation was expressed as a percentage of the total input chromatin. Percent input = 2% × 2 (C[T] 2% input sample - C[T] IP sample), C[T]=$C_T$=Threshold cycle of PCR reaction. The primer sequences are shown in Supplementary Table 1.

### 2.14. Determination of MDA levels of kidney tissue

MDA activity assay kits were used to detect MDA levels in kidney tissues as per the manufacturer's protocols (Nanjing Jiancheng Bioengineering Institute, C013-2-1, Nanjing, China). MDA contents were detected at 450 nm. MDA concentration was normalized by total protein concentration, which was measured using the Bradford method.

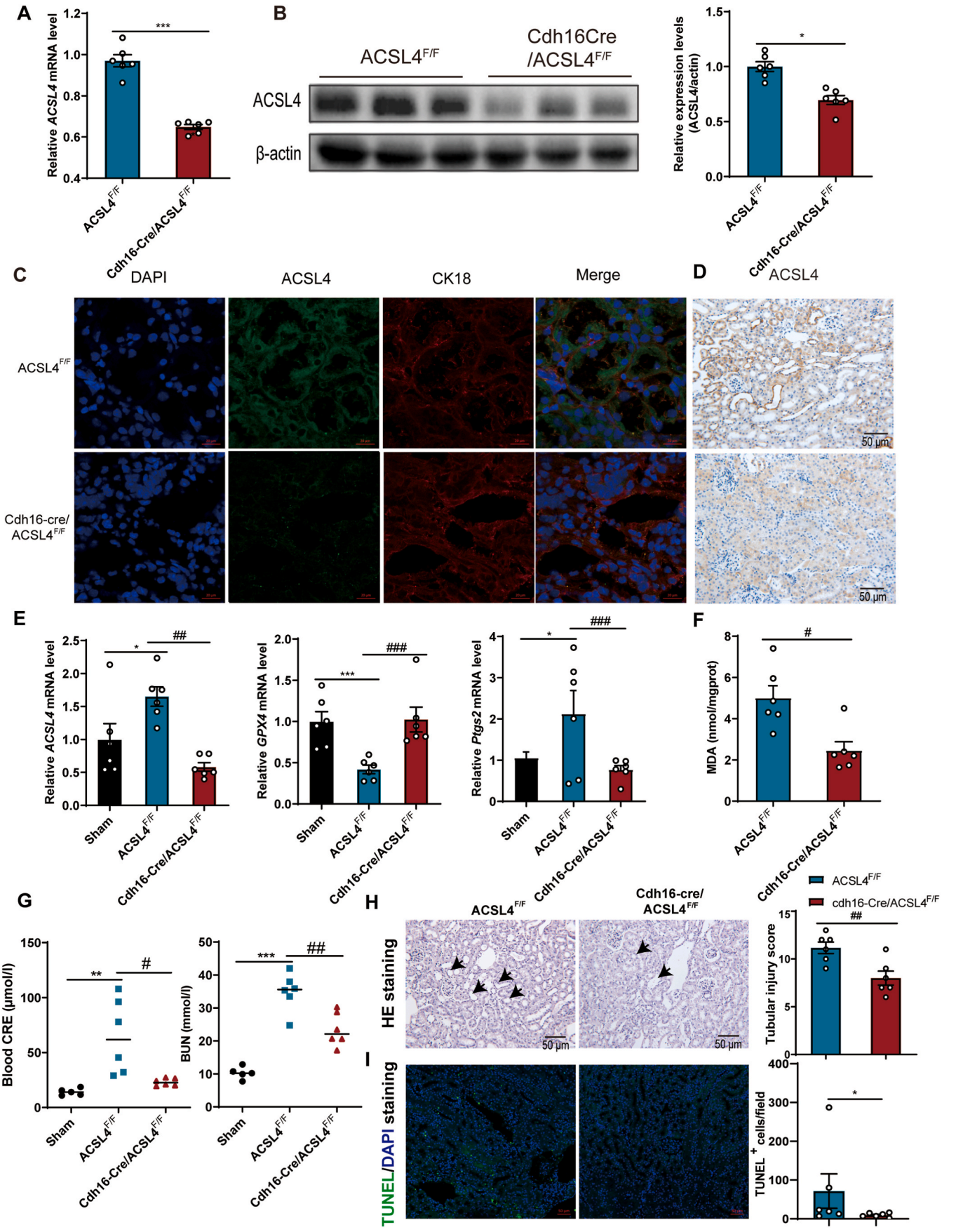


*(caption on next page)*

**Fig. 3.** Knockout of renal ACSL4 has a protective effect on AKI. (A–B) The knockout efficiency of ACSL4 in normal mice kidney examined using RT-PCR and Western blot. N=6. (C) Representative ACSL4 and CK18 immunofluorescent staining pictures in the kidney tissues of Cdh16Cre/ACSL4$^{F/F}$ and ACSL4$^{F/F}$ normal mice. (D) Representative ACSL4 immunohistochemical staining in the kidney tissues of Cdh16Cre/ACSL4$^{F/F}$ and ACSL4$^{F/F}$ mice after AKI. (E) The expression levels of ferroptosis markers *GPX4*, *Ptgs2,* and *ACSL4* in Cdh16Cre/ACSL4$^{F/F}$ and ACSL4$^{F/F}$ mice detected by RT-PCR. N=6. (F) The levels of MDA in kidney tissue of Cdh16Cre/ACSL4$^{F/F}$ and ACSL4$^{F/F}$ mice after AKI. N=5–6. (G) The blood CRE and BUN content of Cdh16Cre/ACSL4$^{F/F}$ and ACSL4$^{F/F}$ mice after AKI. N=6. (H) HE staining of Cdh16Cre/ACSL4$^{F/F}$ and ACSL4$^{F/F}$ mice after AKI. N=6. (I) TUNEL staining of Cdh16Cre/ACSL4$^{F/F}$ and ACSL4$^{F/F}$ mice after AKI. N=6. *$p < 0.05$, **$p < 0.01$, ***$p < 0.001$, compared to Sham group; #$p < 0.05$, ##$p < 0.01$, ###$p < 0.001$, compared to ACSL4$^{F/F}$ group.

### 2.15. Cell isolation and flow cytometry

Kidneys were cut into 1–2 mm$^3$ pieces, incubated in DMEM containing 2 mg/ml Collagenase Type I at 37 °C for 30 min as previously described [34]. Then the cell suspension was filtered through a BD cell strainer (40 μm). Antibodies used for kidney immune cells were as follows: CD45 (FITC), CD11b (PE), Ly6G (PECY7), CD4 (APC), CD8 (PECY7), F4/80 (FITC). Cells were analyzed using the MACSQuant Analyzer 10 (Miltenyi Biotec). Flow cytometry analysis was conducted using the FlowJo software.

### 2.16. Macrophage phagocytosis experiment

Phagocytosis was detected through flow cytometry as previously reported [35]. 52E cells were transfected with labeled GFP lentivirus, then co-incubated with iBMDM cells for 2 h. Macrophages were incubated using PE-labeled CD11b antibody and detected through flow cytometry.

### 2.17. Neutrophil migration assay

Neutrophils were extracted from the femur and tibia of mice. Briefly, the bone marrow cells were extracted with PBS, then incubated with RBC lysate, and centrifuged at 2000 rpm for 5 min. Eventually, neutrophils were harvested through density gradient centrifugation with 81% and 62% percoll solutions. Neutrophils ($1 \times 10^6$ cells) were seeded in the top chamber, and the ferroptotic cells (52E cells treated with Era) and iBMDMs ($5 \times 10^5$ cells) were seeded in the bottom chamber. Migrated cells were counted using Image J.

### 2.18. Statistical analysis

Statistical analysis was conducted using the GraphPad Prism 8.3.0 and data were presented as the mean ± SEM. Student's t-test between two groups or one-way ANOVA followed by Dunnett's post hoc test in groups of more than two was used to establish statistical significance. Correlation analysis was performed using the Pearson correlation statistical analysis. $P < 0.05$ was considered statistically significant.

## 3. Results

### 3.1. ACSL4 is highly expressed in AKI kidney tissues

Ferroptosis promotes AKI [7,19,36], nonetheless, its mechanism is unclear. Herein, RNA-seq sequencing results showed that among the several key pathway genes related to ferroptosis, like glutathione peroxidase 4 (GPX4), ferroptosis suppressor protein 1 (FSP1), ACSL4, and voltage dependent anion channels 2 and 3 (VDAC2/3), only ACSL4 was upregulated in AKI kidney tissues of I/R-induced mice (Fig. 1A). Q-PCR, WB, and immunohistochemistry were used to detect ACSL4 expression levels. Consistently, both the mRNA and protein levels of ACSL4 were upregulated in the kidney tissue of both I/R and FA-induced AKI mice, specifically in the renal tubular cells (Fig. 1B–E). Moreover, the mRNA levels of ACSL4 were significantly and positively correlated with BUN and blood CRE in both FA-AKI and I/R-AKI mice (Fig. 1F and G). Therefore, ACSL4 is highly expressed in AKI and positively correlated with AKI severity.

### 3.2. HIF-1α binds to ACSL4 promoter and negatively regulates ACSL4

The RNA-seq data were re-analyzed to assess the pathway mechanism of ACSL4 in AKI. The results showed that the HIF-1 signaling pathway was enriched (Fig. 2A). HIF-1 signal is widely reported in AKI. Moreover, agonists of HIF-1α inhibit AKI [37–41]. WB and RT-PCR analyses showed that HIF-1α and HIF-2α were down-regulated in AKI, while the ACSL4 levels were upregulated (Fig. 2B). Hypoxia (1% $O_2$) was then used to induce HIF expression and explore its effect on ACSL4. The hypoxia upregulated the protein and mRNA levels of both HIF-1α and HIF-2α, while it downregulated the levels of ACSL4 (Fig. 2C and D). Then, HIF-1α and HIF-2α knockdown in HK-2 cells were constructed, and the knockdown efficacies were confirmed in both mRNA and protein levels. Besides, the mRNA level of aryl hydrocarbon receptor nuclear translocator (ARNT), the HIF-1α/2α partner protein, was not knocked down by shHIF-1α/2α, but slightly and maybe compensatorily increased (Fig. S1). Nonetheless, only the knockdown of HIF-1α significantly upregulated the expression level of ACSL4 (Fig. 2E and F). Similarly, BAY 87-2243-a, HIF-1α inhibitor, upregulated the ACSL4 mRNA levels. However, PT2385, HIF-2α inhibitor, did not upregulate ACSL4 mRNA levels (Fig. 2G). Furthermore, HIF-1α knockdown upregulated HK-2 cell susceptibility to ferroptosis while inhibitor of ACSL4 reversed its effect (Fig. 2H). Also, the mRNA levels of *CCL2* were increased by HIF-1α knockdown (Fig. 2I). A chromatin immunoprecipitation assay was conducted to explore the mechanism underlying the regulation of HIF-1α on ACSL4. The HIF-1α overexpression plasmid was first transfected into HK-2 cells. The luciferase experiment showed that HIF-1α inhibited ACSL4 expression (Fig. 2J). Then, the cytoplasm and nucleus of HK-2 cells were isolated at 21% $O_2$ or 1% $O_2$ conditions. As a consequence, HIF-1α and ACSL4 were expressed in the nucleus and cytoplasm, respectively (Fig. 2K). Finally, the Chip experiment revealed that HIF-1α could bind to the promoter of ACSL4 and disrupt ACSL4 expression (Fig. 2L). In summary, the results showed that HIF-1α could bind to ACSL4 promoter and negatively regulate ACSL4. The downregulated expression of HIF-1α in AKI may cause the high expression of ACSL4, thereby inducing ferroptosis.

### 3.3. ACSL4 knockout protects the kidney in I/R-induced AKI

ACSL4 renal tubular conditional knockout mice were developed to investigate the role of ACSL4 in AKI. The ACSL4 knockout efficacy was confirmed, and the results showed that the expression levels of ACSL4 protein and mRNA in the kidney tissues were significantly downregulated in Cdh16Cre-ACSL4$^{F/F}$ mice compared to that in ACSL4$^{F/F}$ mice (Fig. 3A and B). The body weight, kidney/spleen/thymus index, levels of BUN, CRE, and blood routine cell changes showed no difference in both Cdh16Cre-ACSL4$^{F/F}$ and ACSL4$^{F/F}$ mice in the normal situation (Figs. S2A–S2D). Then, I/R-induced AKI was conducted in ACSL4$^{F/F}$ and Cdh16Cre-ACSL4$^{F/F}$ mice. Immunofluorescent staining, immunohistochemical staining, and PCR results showed downregulated ACSL4 expression level in the kidney of Cdh16Cre-ACSL4$^{F/F}$ mice, particularly in tubular epithelial cells, since ACSL4 was colocalized with tubular epithelial marker Cytokeratin18 (CK18) (Fig. 3C, D and 3E). The expression levels of *GPX4* and *Ptgs2* mRNA were upregulated and downregulated respectively in Cdh16Cre-ACSL4$^{F/F}$ mice (Fig. 3E). Inactivation of GPX4, an essential antioxidant peroxidase directly causes ferroptosis [42]. While Ptgs2 is also a known increased marker in ferroptosis [43,44]. Therefore, these results confirm the inhibition of

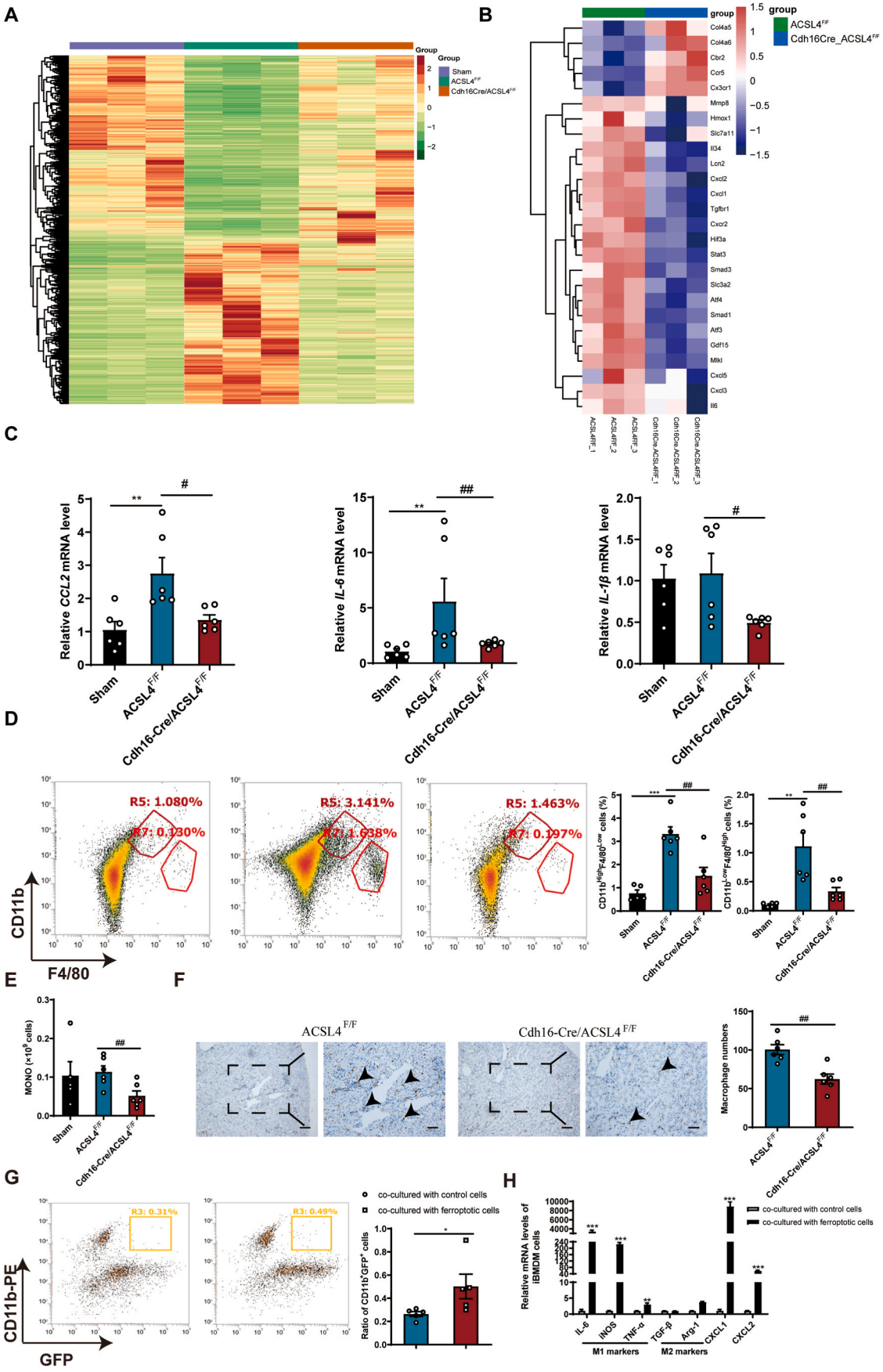


*(caption on next page)*

**Fig. 4.** Knockdown of renal ACSL4 inhibits the release of renal inflammatory factors. (A) The heatmap of RNA-seq in the kidney of three groups. N=3. (B) A heatmap showing the differentially expressed genes related to inflammatory responses in ACSL4$^{F/F}$ and Cdh16Cre/ACSL4$^{F/F}$ groups. N=3. (C) RT-PCR analysis of *CCL2*, *IL-6,* and *IL-1β* mRNA in kidney tissues of three groups. N=6. (D) The proportion of macrophages in the kidney tissue of mice detected by flow cytometry. N=6. (E) The blood mononuclear detected through blood routine detection. N=6. (F) Staining of macrophages in kidney tissue. The scale bars represent 100 μm and 50 μm. N=6. (G) Flow cytometry analysis of macrophages phagocytosis of control or ferroptotic cells. Ferroptosis was induced by Erastin. N=6. (H) The mRNA expression of *IL-6*, *iNOS*, *TNF-α*, *TGF-β*, *Arg-1*, *CXCL1,* and *CXCL2* in macrophages after co-incubation with ferroptotic cells. N=4. $*p < 0.05$, $**p < 0.01$, $***p < 0.001$, compared to the Sham group; $\#p < 0.05$, $\#\#p < 0.01$, $\#\#\#p < 0.001$, compared with the ACSL4$^{F/F}$ group.

ferroptosis in Cdh16Cre-ACSL4$^{F/F}$ mice. Furthermore, the lipid oxidation product MDA content was significantly reduced in kidney tissue of Cdh16Cre-ACSL4$^{F/F}$ mice (Fig. 3F) The contents of BUN and blood CRE were significantly decreased (Fig. 3G). Besides, the pathological damage of the kidney was alleviated in Cdh16Cre-ACSL4$^{F/F}$ mice (Fig. 3H), as well as dead cells stained with TUNEL (Fig. 3I), indicates a protective effect of ACSL4 knockout on I/R-induced AKI. Thus, ACSL4 knockout in renal tubular inhibits I/R-induced AKI by targeting ferroptosis.

### 3.4. *Cdh16Cre-ACSL4$^{F/F}$ inhibits the inflammatory reaction in I/R-induced AKI*

Despite tubular cell death, inflammation is also considered a key player in AKI [7]. Ferroptosis is a pro-inflammatory agent and recruits macrophages, causing inflammation in AKI [22]. Herein, RNA sequence analysis revealed that gene levels were significantly changed in the ACSL4$^{F/F}$ I/R group. In contrast, the gene levels were normal in the Cdh16Cre-ACSL4$^{F/F}$ group (Fig. 4A). Cdh16Cre-ACSL4$^{F/F}$ decreased the high levels of inflammatory factors, including *Mmp8*, *Hmox1*, *Lcn2*, *Cxcl2*, *Cxcl1*, *Stat3*, *Cxcl3*, *IL-6* (Fig. 4B). The signaling pathways of differentially expressed genes were cytokine-cytokine receptor interaction and TNF signaling pathways (Fig. S3). RT-PCR results showed that the mRNA levels of chemokines (*CCL2*) and inflammatory factors (*IL-1β* and *IL-6*) were significantly reduced in the kidney tissue of Cdh16Cre-ACSL4$^{F/F}$ mice (Fig. 4C). Flow cytometry analysis showed that the infiltration of CD11b$^{+}$F4/80$^{+}$ macrophages was significantly reduced in the kidneys of Cdh16Cre-ACSL4$^{F/F}$ mice (Fig. 4D). Also, routine blood tests and immunohistochemical experiments showed lower monocytes and less infiltration of macrophages in the kidney of Cdh16Cre-ACSL4$^{F/F}$ mice (Fig. 4E and F). Collectively, consistent with previous findings, the results show that ACSL4 knockout reduces inflammation and macrophage aggregation in the kidney of I/R-induced mice [22].

Although ferroptotic cells recruit macrophages [22], the role of ferroptotic cells in macrophages is unclear. Flow cytometry was used to detect macrophage phagocytosis on ferroptotic cells (Fig. S4). Consequently, macrophages phagocytized several ferropotic cells (Fig. 4G). Further, ferroptotic cells significantly caused M1 polarization of macrophages, upregulating the M1 macrophage markers, including *IL-6*, *iNOS*, and *TNF-α* (Fig. 4H). Moreover, *CXCL1* and *CXCL2*, the major neutrophil chemokines, were substantially increased in macrophages co-cultured with ferroptotic cells (Fig. 4H).

### 3.5. *Ferroptotic cells induce macrophages to recruit neutrophils*

In addition to macrophages, neutrophils are inflammatory cells and promote AKI [45–47]. Neutrophil chemokines were significantly increased in AKI and decreased in Cdh16Cre-ACSL4$^{F/F}$ mice (Figs. 4B and 5A). Also, flow cytometry, routine blood test, and immunohistochemical experiment confirmed the downregulating effect of Cdh16Cre-ACSL4$^{F/F}$ on neutrophils (Fig. 5B–D). Therefore an in vitro chemotaxis experiment was conducted using ferroptotic cells and neutrophils to identify whether neutrophils are also recruited by ferroptotic cells. However, neutrophils were not recruited by ferroptotic cells (Fig. 5E). Besides, chemokines were not induced by ferroptotic cells (Fig. 5F). Reports indicate that macrophages release chemokines to recruit granulocytes to the injury site [48]. So, ferroptotic cells might induce macrophages to recruit neutrophils due to the upregulated expression levels of CXCL1 and CXCL2 by ferroptotic cells-induced macrophages (Fig. 4H). *In vitro* chemotaxis experiment also showed neutrophil recruitment by macrophages (Fig. 5G). Furthermore, ferroptosis inhibitor Fer-1 downregulated the expression levels of *CXCL1*, *CXCL2,* and neutrophil infiltration in the kidney (Fig. 5H and I) in vivo. Therefore, ferroptotic cells indirectly recruit neutrophils, providing another pro-inflammatory effect of ferroptosis in AKI. Nonetheless, Cdh16Cre-ACSL4$^{F/F}$ effectively inhibits this pro-inflammatory effect.

### 3.6. *ACSL4 inhibitor rosiglitazone (Rosi) protects the renal function of AKI by inhibiting ferroptosis and inflammation*

ACSL4 inhibitor Rosi was administered to further confirm the role of ACSL4 in AKI. As a consequence, lower blood CRE, kidney index, and alleviated pathological kidney damage in the I/R+Rosi group (Fig. 6A–C). Additionally, TUNEL staining showed a decrease of Rosi on kidney cell death (Fig. S5). Consistently, Rosi downregulated the levels of *ACSL4*, *CCL2*, *CXCL1,* and *CXCL2* (Fig. 6D). Immunohistochemistry and flow cytometry revealed less renal macrophage infiltration in the I/R+Rosi group (Fig. 6E and F). In general, these findings indicate that Rosi has a protective effect on AKI and reduces the infiltration of inflammatory cells, indicating the crucial role of ACSL4 in AKI.

## 4. Discussion

This study demonstrated that ferroptosis is implicated in the inflammatory responses of kidneys in AKI, and ACSL4 is the primary trigger for ferroptosis in AKI. ACSL4 inhibition protects the kidney from I/R-induced kidney injury. Previous studies reported that AKI is associated with apoptosis [49,50], necrosis [12,51], and autophagy [52,53]. However, our work and previous studies have confirmed that ferroptosis is a potential pathway in the pathology of AKI [18,22,54]. Studies on kidney tubular cell lines treated with tertbutyl hydroperoxide [55] as well as freshly isolated tubules treated with iron and hydroxyquinoline reveal that ferrostatin-1 substantially increased cellular survival [56]. Besides, experiments revealed that lack of ferritin heavy chain in proximal tubular cells worse renal injury, suggesting that iron is involved in the pathophysiology of AKI [57]. Moreover, among 60 cancer cell lines that induced ferroptosis with erastin, renal cell carcinomas are the most sensitive [42]. Therefore, ferroptosis is a potential therapeutic target for diseases contributed by kidney tubular death, including ischemic, cisplatin nephrotoxic, and rhabdomyolysis-induced AKI [58–60].

ACSL4 is related to cell death sensitivity and is considered as a ferroptosis maker [25,26]. In line with previous studies, we also found that ACSL4 is upregulated in the kidney tissue of AKI through analysis of kidney RNA-seq and other experiments. Then, we selected the Cdh16Cre mouse to knock out ACSL4 in tubules. Besides, ACSL4$^{F/F}$ and Cdh16Cre-ACSL4$^{F/F}$ mice were similar in normal conditions. Nevertheless, genetic knockout of ACSL4 and ACSL4 inhibitor rosiglitazone significantly improved renal function, inhibited pathological kidney damage, as well as decreased inflammatory factors and immune cell infiltration in the kidney of the I/R-induced AKI group. This indicates that ACSL4 prevents and treats AKI. Nonetheless, rosiglitazone has been restricted due to its significant adverse reactions during its clinical use. Therefore, it is necessary to explore a novel compound in the future [61,62].

KEGG analysis of kidney tissues revealed that HIF-1 signaling pathways between CON and I/R groups were significantly different. Previous

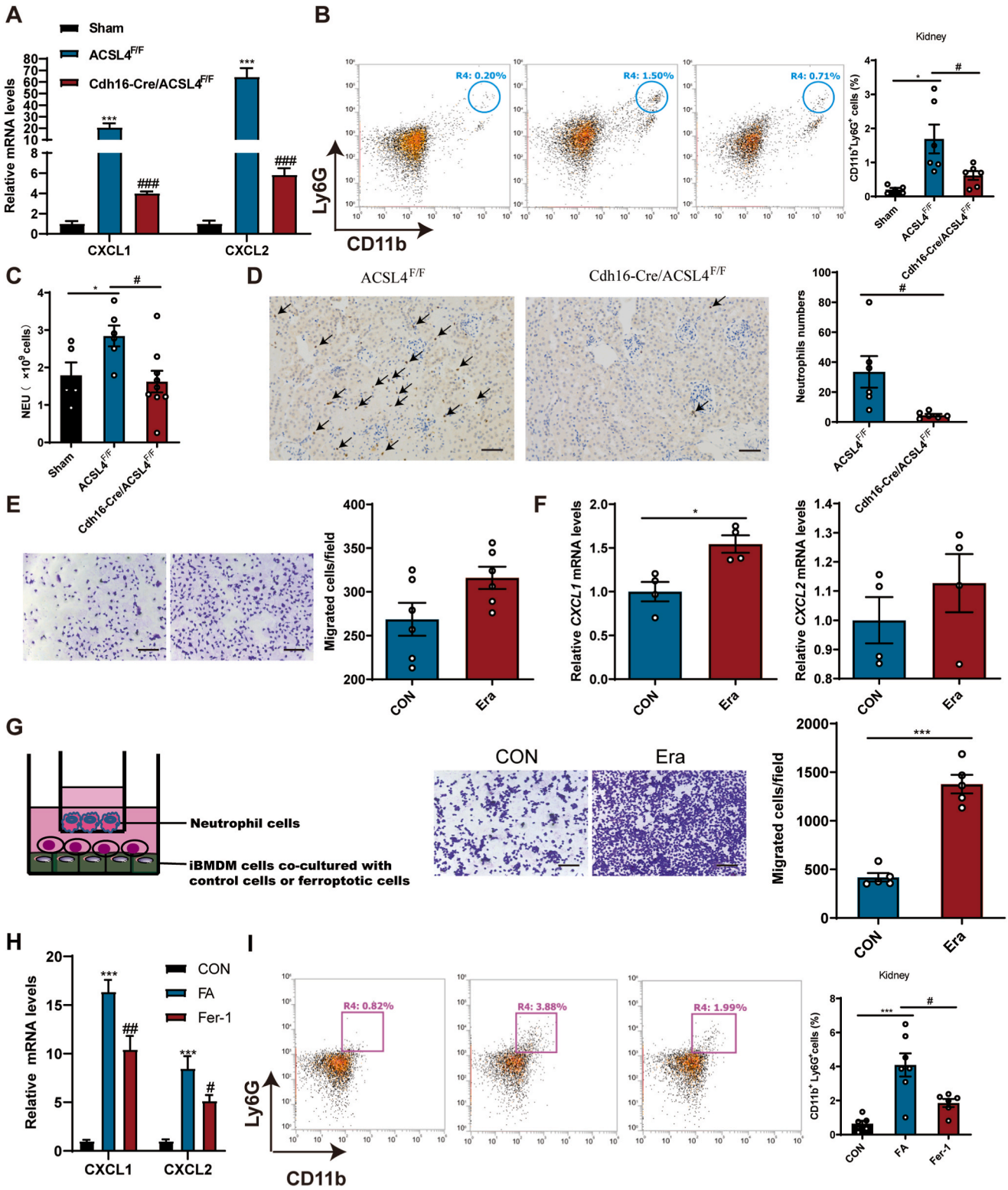


**Fig. 5.** Macrophages recruit neutrophils by secreting neutrophil chemokines. (A) RT-PCR analysis of *CXCL1* and *CXCL2* in kidney tissue of three groups. N=4. (B) Flow cytometry statistics of $CD11b^{+}Ly6G^{+}$ neutrophils in the kidney of three groups. N=6. (C–D) Blood routine test and immunohistochemical staining showing neutrophil expressions in the kidney of mice. The MPO antibody was stained in the kidney to indicate the neutrophil. The scale bars represent 50 μm. N=6. (E) The migrated neutrophils with crystal violet staining induced by ferroptotic 52E cells. N=3. (F) The expression of *CXCL1* and *CXCL2* mRNA levels in ferroptotic 52E cells. N=4. (G) The migrated neutrophils with crystal violet staining induced by macrophages and control or ferroptotic 52E cells. N=3. (H) RT-PCR results of *CXCL1*and *CXCL2* in the mice kidneys. N=6. (I) Flow cytometry and analysis of $CD11b^{+}Ly6G^{+}$ neutrophil cells in the mice kidneys. N=6. $^{*}p < 0.05$, $^{***}p < 0.001$, compared to sham or CON group; $\#p < 0.05$, $\#\#\#p < 0.001$, compared with $ACSL4^{F/F}$ or FA groups. (For interpretation of the references to colour in this figure legend, the reader is referred to the Web version of this article.)

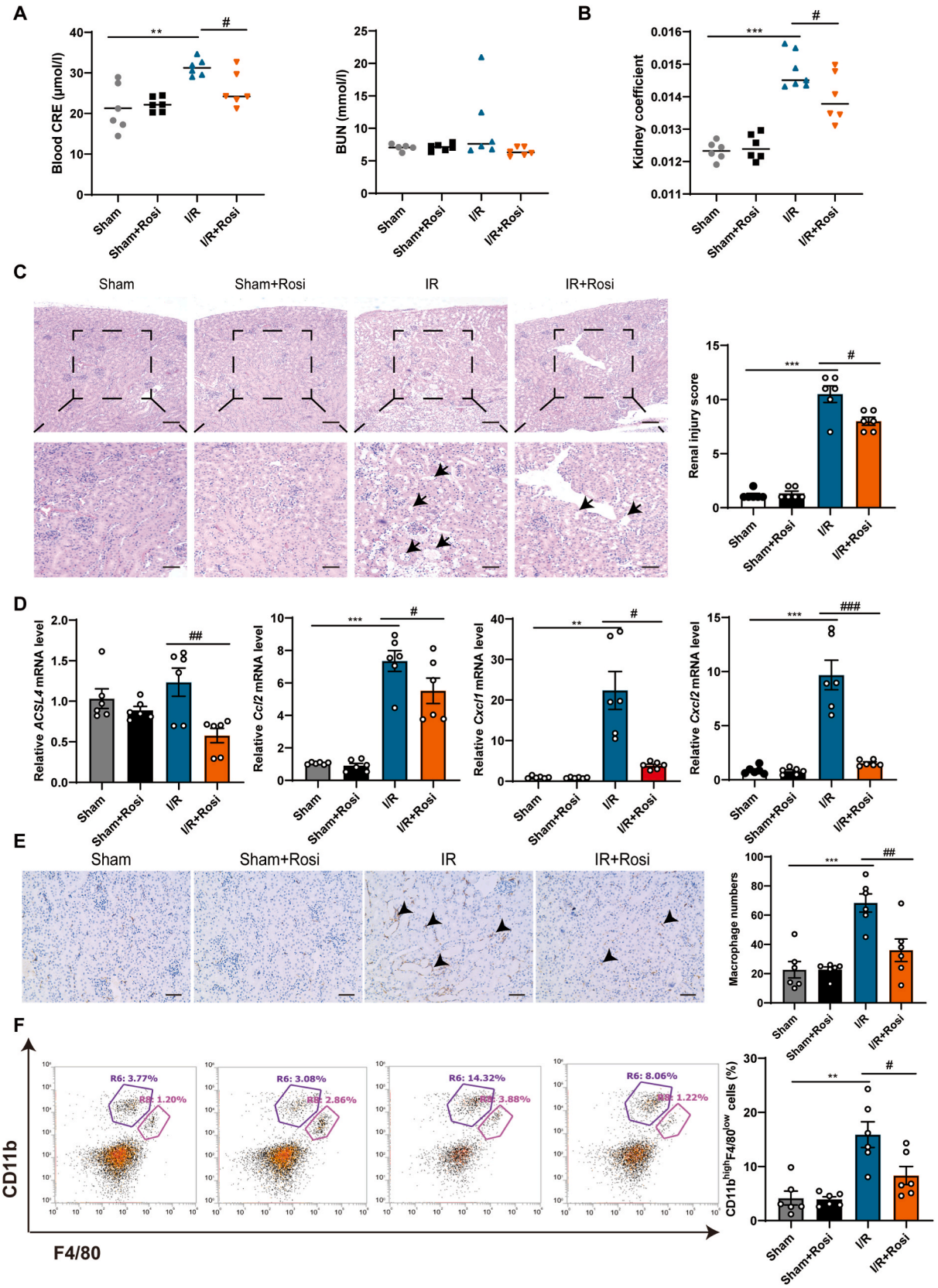


**Fig. 6.** ACSL4 inhibitor rosiglitazone (Rosi) protects the renal function of AKI by inhibiting ferroptosis and inflammation. (A–B) BUN and blood CRE levels and kidney coefficient in mice. (C) Representative HE staining and pathological scores of the kidneys. The scale bars represent 50 μm and 100 μm. (D) RT-PCR results of *ACSL4*, *CCL2*, *CXCL1*, and *CXCL2* in mice kidneys. (E) Representative F4/80 staining images and mean F4/80 positive cells in the kidney. The scale bar represents 50 μm. (F) The ratio of $CD11b^{+}F4/80^{+}$ macrophage cells in the kidney tissue of I/R-induced AKI detected by flow cytometry. $^{**}p < 0.01$, $^{***}p < 0.001$, compared to Sham group; $\#p < 0.05$, $\#\#p < 0.01$, $\#\#\#p < 0.001$, compared to I/R group. N=6.

studies demonstrated that the HIF pathway is involved in kidney injury and AKI repair [37,63]. HIF prolyl hydroxylases inhibitor FG-4592 or recombinant HIF-1α protein treatment significantly ameliorates AKI kidney injury by improving renal function and kidney morphology [40,64]. HIF-1α and HIF-2α were downregulated in the I/R-induced AKI model, while ACSL4 was upregulated. During hypoxia, ACSL4 in both 52E cells and HK-2 cells was significantly downregulated, accompanied by upsurges of HIF-1α and HIF-2α. However, knockdown of HIF-1α but not HIF-2α upregulated the expression level of ACSL4, indicating a negative regulation of HIF-1α on ACSL4. As expected, knockdown of HIF-1α rendered cells susceptible to erastin-induced ferroptosis. For the mechanism behind the regulation of HIF-1α on ACSL4, we found that HIF-1α could bind to the promoter of ACSL4 and may regulate ACSL4. HIF-1α is known as a transcriptionally active nuclear protein with a broad target gene spectrum, including nearly 100 target genes related to hypoxia adaptation, inflammation development and tumor growth. We only found the binding of HIF-1α on the ACSL4 promoter, However, the comprehensive mechanism by which this combination inhibits the expression warrants further exploration. This finding suggests an interesting concept that activation of HIF-1α may ease AKI, which also effectively fits well with evidence and discussion before HIF-1α upregulation becomes beneficial to AKI [40].

Various cell deaths release and activate different damage-related molecular patterns (DAMP) signals, thereby initiating a signal cascade and promoting the release of several inflammatory factors. This triggers a strong inflammatory response, and in turn a vicious cycle between cell death and inflammation [65]. RNA-sequence showed that several inflammation-related genes are significantly upregulated in kidney tissue of mice in the I/R group. We previously found that ferroptotic cells recruit macrophages by secreting CCL2 [22]. Moreover, ferroptotic cells polarized macrophages into M1 types. In the kidney of AKI, macrophages and neutrophils were increased. However, neutrophils could not be directly recruited by ferroptotic cells. Interestingly, ferroptotic cells could induce macrophages to release CXCL1 and CXCL2, which then aggregated neutrophils in the kidney. Inhibition of ferroptosis could block both the infiltration of macrophages and neutrophils in AKI mice kidneys. These findings further unravel the mystery of cell death-induced inflammation.

In conclusion, this study shows ACSL4 knockout prevents AKI by inhibiting ferroptosis and inflammation. We found that (i) ACSL4 is a potential target in preventing and treating AKI by inhibiting ferroptosis; (ii) HIF-1α binds to the promoter of ACSL4 and negatively regulates its expression; (iii) Ferroptotic cells recruit macrophages and stimulate macrophages to recruit neutrophils, thereby causing an inflammatory cascade reaction in AKI. Our findings provide a reference for the development of novel therapeutic approaches for AKI and ferroptosis-related diseases.

## Author contributions

X.G., Y.W., and Q.C. designed research; Y.W., Q.C., R.B., M.Z., F.Q., Y.L., C.Y., X.C. Q.Z., S.L., Y.S., and X.G. performed research; Y.W. and X. G. analyzed data; Y.Y., D.Z., M.Z., Y.W., and X.G. wrote the paper.

## Declaration of competing interest

The authors declare no competing financial interests.

## Acknowledgments

This work was supported by National Natural Science Foundation of China grants (82072720).

## Appendix A. Supplementary data

Supplementary data to this article can be found online at https://doi.org/10.1016/j.redox.2022.102262.

## References

[1] N.H. Lameire, A. Bagga, D. Cruz, et al., Acute kidney injury: an increasing global concern, Lancet 382 (2013) 170–179.
[2] A.J. Lewington, J. Cerda, R.L. Mehta, Raising awareness of acute kidney injury: a global perspective of a silent killer, Kidney Int. 84 (2013) 457–467.
[3] A.S. Levey, M.T. James, Acute kidney injury, Ann. Intern. Med. 167 (2017) ITC66–ITC80.
[4] E.D. Siew, S.K. Parr, K. Abdel-Kader, et al., Predictors of recurrent AKI, J. Am. Soc. Nephrol. 27 (2016) 1190–1200.
[5] N. Pannu, M.K. Nadim, An overview of drug-induced acute kidney injury, Crit. Care Med. 36 (2008) S216–S223.
[6] J.V. Bonventre, L. Yang, Cellular pathophysiology of ischemic acute kidney injury, J. Clin. Invest. 121 (2011) 4210–4221.
[7] A. Linkermann, G. Chen, G. Dong, et al., Regulated cell death in AKI, J. Am. Soc. Nephrol. 25 (2014) 2689–2701.
[8] G.P. Kaushal, A.B. Singh, S.V. Shah, Identification of gene family of caspases in rat kidney and altered expression in ischemia-reperfusion injury, Am. J. Physiol. 274 (1998) F587–F595.
[9] P. Li, M. Shi, J. Maique, et al., Beclin 1/Bcl-2 complex-dependent autophagy activity modulates renal susceptibility to ischemia-reperfusion injury and mediates renoprotection by Klotho, Am. J. Physiol. Ren. Physiol. 318 (2020) F772–F792.
[10] A. Linkermann, J.H. Brasen, N. Himmerkus, et al., Rip1 (receptor-interacting protein kinase 1) mediates necroptosis and contributes to renal ischemia/reperfusion injury, Kidney Int. 81 (2012) 751–761.
[11] A. Linkermann, J.H. Brasen, M. Darding, et al., Two independent pathways of regulated necrosis mediate ischemia-reperfusion injury, Proc. Natl. Acad. Sci. U. S. A. 110 (2013) 12024–12029.
[12] Y. Xu, H. Ma, J. Shao, et al., A role for tubular necroptosis in cisplatin-induced AKI, J. Am. Soc. Nephrol. 26 (2015) 2647–2658.
[13] Z. Wang, Z. Gu, Q. Hou, et al., Zebrafish GSDMEb cleavage-gated pyroptosis drives septic acute kidney injury in vivo, J. Immunol. 204 (2020) 1929–1942.
[14] S. Jiang, H. Zhang, X. Li, et al., Vitamin D/VDR attenuate cisplatin-induced AKI by down-regulating NLRP3/Caspase-1/GSDMD pyroptosis pathway, J. Steroid Biochem. Mol. Biol. 206 (2021) 105789.
[15] C. Xiao, H. Zhao, H. Zhu, et al., Tisp40 induces tubular epithelial cell GSDMD-mediated pyroptosis in renal ischemia-reperfusion injury via NF-kappaB signaling, Front. Physiol. 11 (2020) 906.
[16] S.J. Dixon, K.M. Lemberg, M.R. Lamprecht, et al., Ferroptosis: an iron-dependent form of nonapoptotic cell death, Cell 149 (2012) 1060–1072.
[17] Y. Xie, W. Hou, X. Song, et al., Ferroptosis: process and function, Cell Death Differ. 23 (2016) 369–379.
[18] A. Linkermann, R. Skouta, N. Himmerkus, et al., Synchronized renal tubular cell death involves ferroptosis, Proc. Natl. Acad. Sci. U. S. A. 111 (2014) 16836–16841.
[19] D. Martin-Sanchez, O. Ruiz-Andres, J. Poveda, et al., Ferroptosis, but not necroptosis, is important in nephrotoxic folic acid-induced AKI, J. Am. Soc. Nephrol. 28 (2017) 218–229.
[20] Z. Hu, H. Zhang, S.K. Yang, et al., Emerging role of ferroptosis in acute kidney injury, Oxid. Med. Cell. Longev. (2019) 8010614.
[21] B. Borawski, J. Malyszko, Iron, ferroptosis, and new insights for prevention in acute kidney injury, Adv. Med. Sci. 65 (2020) 361–370.
[22] Y. Wang, F. Quan, Q. Cao, et al., Quercetin alleviates acute kidney injury by inhibiting ferroptosis, J. Adv. Res. 28 (2021) 231–243.
[23] Z. Hu, H. Zhang, B. Yi, et al., VDR activation attenuate cisplatin induced AKI by inhibiting ferroptosis, Cell Death Dis. 11 (2020) 73.
[24] Z. Zhao, J. Wu, H. Xu, et al., XJB-5-131 inhibited ferroptosis in tubular epithelial cells after ischemia-reperfusion injury, Cell Death Dis. 11 (2020) 629.
[25] H. Yuan, X. Li, X. Zhang, et al., Identification of ACSL4 as a biomarker and contributor of ferroptosis, Biochem. Biophys. Res. Commun. 478 (2016) 1338–1343.
[26] S. Doll, B. Proneth, Y.Y. Tyurina, et al., ACSL4 dictates ferroptosis sensitivity by shaping cellular lipid composition, Nat. Chem. Biol. 13 (2017) 91–98.
[27] Y. Zhao, J. Yang, J. Shi, et al., The NLRC4 inflammasome receptors for bacterial flagellin and type III secretion apparatus, Nature 477 (2011) 596–600.
[28] H. Xu, J. Yang, W. Gao, et al., Innate immune sensing of bacterial modifications of Rho GTPases by the Pyrin inflammasome, Nature 513 (2014) 237–241.
[29] J. Shi, Y. Zhao, K. Wang, et al., Cleavage of GSDMD by inflammatory caspases determines pyroptotic cell death, Nature 526 (2015) 660–665.
[30] V. Hornung, F. Bauernfeind, A. Halle, et al., Silica crystals and aluminum salts activate the NALP3 inflammasome through phagosomal destabilization, Nat. Immunol. 9 (2008) 847–856.
[31] V. Vichai, K. Kirtikara, Sulforhodamine B colorimetric assay for cytotoxicity screening, Nat. Protoc. 1 (2006) 1112–1116.
[32] E.C. Lien, C.A. Lyssiotis, A. Juvekar, et al., Glutathione biosynthesis is a metabolic vulnerability in PI(3)K/Akt-driven breast cancer, Nat. Cell Biol. 18 (2016) 572–578.
[33] J.R. Liu, Q. Liu, J. Li, et al., Noxious stimulation attenuates ketamine-induced neuroapoptosis in the developing rat brain, Anesthesiology 117 (2012) 64–71.
[34] R. Bethunaickan, C.C. Berthier, M. Ramanujam, et al., A unique hybrid renal mononuclear phagocyte activation phenotype in murine systemic lupus erythematosus nephritis, J. Immunol. 186 (2011) 4994–5003.
[35] A.A. Barkal, R.E. Brewer, M. Markovic, et al., CD24 signalling through macrophage Siglec-10 is a target for cancer immunotherapy, Nature 572 (2019) 392–396.

[36] A. Linkermann, R. Skouta, N. Himmerkus, et al., Synchronized renal tubular cell death involves ferroptosis, Proc. Natl. Acad. Sci. U. S. A. 111 (2014) 16836–16841.
[37] S. Shu, Y. Wang, M. Zheng, et al., Hypoxia and hypoxia-inducible factors in kidney injury and repair, Cells 8 (2019).
[38] G. Rajendran, M.P. Schonfeld, R. Tiwari, et al., Inhibition of endothelial PHD2 suppresses post-ischemic kidney inflammation through hypoxia-inducible factor-1, J. Am. Soc. Nephrol. 31 (2020) 501–516.
[39] J. Günter, R.H. Wenger, C.C. Scholz, Inhibition of firefly luciferase activity by a HIF prolyl hydroxylase inhibitor, J. Photochem. Photobiol., B 210 (2020) 111980.
[40] Y. Yang, X. Yu, Y. Zhang, et al., Hypoxia-inducible factor prolyl hydroxylase inhibitor roxadustat (FG-4592) protects against cisplatin-induced acute kidney injury, Clin. Sci. (Lond.) 132 (2018) 825–838.
[41] Z.J. Fu, Z.Y. Wang, L. Xu, et al., HIF-1α-BNIP3-mediated mitophagy in tubular cells protects against renal ischemia/reperfusion injury, Redox Biol. 36 (2020) 101671.
[42] W.S. Yang, R. SriRamaratnam, M.E. Welsch, et al., Regulation of ferroptotic cancer cell death by GPX4, Cell 156 (2014) 317–331.
[43] X.Y. Mao, H.H. Zhou, W.L. Jin, Ferroptosis induction in pentylenetetrazole kindling and pilocarpine-induced epileptic seizures in mice, Front. Neurosci. 13 (2019) 721.
[44] N. Yamada, T. Karasawa, H. Kimura, et al., Ferroptosis driven by radical oxidation of n-6 polyunsaturated fatty acids mediates acetaminophen-induced acute liver failure, Cell Death Dis. 11 (2020) 144.
[45] H. Block, J.M. Herter, J. Rossaint, et al., Crucial role of SLP-76 and ADAP for neutrophil recruitment in mouse kidney ischemia-reperfusion injury, J. Exp. Med. 209 (2012) 407–421.
[46] B. Deng, Y. Lin, S. Ma, et al., The leukotriene B(4)-leukotriene B(4) receptor axis promotes cisplatin-induced acute kidney injury by modulating neutrophil recruitment, Kidney Int. 92 (2017) 89–100.
[47] H.R. Jang, H. Rabb, Immune cells in experimental acute kidney injury, Nat. Rev. Nephrol. 11 (2015) 88–101.
[48] K. Prame Kumar, A.J. Nicholls, C.H.Y. Wong, Partners in crime: neutrophils and monocytes/macrophages in inflammation and disease, Cell Tissue Res. 371 (2018) 551–565.
[49] M.Z. Zhang, B. Yao, S. Yang, et al., CSF-1 signaling mediates recovery from acute kidney injury, J. Clin. Invest. 122 (2012) 4519–4532.
[50] Q. Wei, H. Sun, S. Song, et al., MicroRNA-668 represses MTP18 to preserve mitochondrial dynamics in ischemic acute kidney injury, J. Clin. Invest. 128 (2018) 5448–5464.
[51] S.R. Mulay, M.M. Honarpisheh, O. Foresto-Neto, et al., Mitochondria permeability transition versus necroptosis in oxalate-induced AKI, J. Am. Soc. Nephrol. 30 (2019) 1857–1869.
[52] G.P. Kaushal, Autophagy protects proximal tubular cells from injury and apoptosis, Kidney Int. 82 (2012) 1250–1253.
[53] L. Zhu, Y. Yuan, L. Yuan, et al., Activation of TFEB-mediated autophagy by trehalose attenuates mitochondrial dysfunction in cisplatin-induced acute kidney injury, Theranostics 10 (2020) 5829–5844.
[54] Y. Li, D. Feng, Z. Wang, et al., Ischemia-induced ACSL4 activation contributes to ferroptosis-mediated tissue injury in intestinal ischemia/reperfusion, Cell Death Differ. 26 (2019) 2284–2299.
[55] G. Nowak, S. Soundararajan, R. Mestril, Protein kinase C-alpha interaction with iHSP70 in mitochondria promotes recovery of mitochondrial function after injury in renal proximal tubular cells, Am. J. Physiol. Ren. Physiol. 305 (2013) F764–F776.
[56] R. Skouta, S.J. Dixon, J. Wang, et al., Ferrostatins inhibit oxidative lipid damage and cell death in diverse disease models, J. Am. Chem. Soc. 136 (2014) 4551–4556.
[57] A. Zarjou, S. Bolisetty, R. Joseph, et al., Proximal tubule H-ferritin mediates iron trafficking in acute kidney injury, J. Clin. Invest. 123 (2013) 4423–4434.
[58] T. Vanden Berghe, A. Linkermann, S. Jouan-Lanhouet, et al., Regulated necrosis: the expanding network of non-apoptotic cell death pathways, Nat. Rev. Mol. Cell Biol. 15 (2014) 135–147.
[59] S.J. Dixon, B.R. Stockwell, The role of iron and reactive oxygen species in cell death, Nat. Chem. Biol. 10 (2014) 9–17.
[60] M. Fähling, S. Mathia, A. Paliege, et al., Tubular von Hippel-Lindau knockout protects against rhabdomyolysis-induced AKI, J. Am. Soc. Nephrol. 24 (2013) 1806–1819.
[61] H.E. Lebovitz, Thiazolidinediones: the forgotten diabetes medications, Curr. Diabetes Rep. 19 (2019) 151.
[62] S.E. Nissen, K. Wolski, Effect of rosiglitazone on the risk of myocardial infarction and death from cardiovascular causes, N. Engl. J. Med. 356 (2007) 2457–2471.
[63] K.K. Andringa, A. Agarwal, Role of hypoxia-inducible factors in acute kidney injury, Nephron Clin. Pract. 127 (2014) 70–74.
[64] H. Wang, N. Liu, R. Li, et al., Nephropreventing effect of hypoxia-inducible factor 1α in a rat model of ischaemic/reperfusion acute kidney injury, Clin. Exp. Pharmacol. Physiol. 45 (2018) 1076–1082.
[65] S.R. Mulay, A. Linkermann, H.J. Anders, Necroinflammation in kidney disease, J. Am. Soc. Nephrol. 27 (2016) 27–39.